

Drag of a Heated Sphere at Low Reynolds Numbers in the Presence of Buoyancy

Swetava Ganguli^{1,2,*} and Sanjiva K. Lele^{1,3}

¹*Department of Mechanical Engineering, Stanford University, Stanford, CA 94305*

²*Department of Computer Science, Stanford University, Stanford, CA 94305*

³*Department of Aeronautics and Astronautics, Stanford University, Stanford, CA 94305*

Fully resolved simulations are used to quantify the effects of heat transfer in the presence of buoyancy on the drag of a spatially fixed heated spherical particle at low Reynolds numbers (Re) in the range $10^{-3} \leq Re \leq 10$ in a variable property fluid, extending the analysis presented in [1]. The amount of heat addition from the sphere encompasses both, the heating regime where the Boussinesq approximation holds and the regime where it breaks down. The particle is assumed to have a low Biot number which means that the particle is uniformly at the same temperature and has no internal temperature gradients. Scaling buoyancy with inertial and viscous forces yields two related non-dimensional quantities, called *Buoyancy Induced Viscous Reynolds Number* (Re_{BV}) and *Buoyancy Induced Inertial Reynolds Number* (Re_{BI}). For ideal gases, Re_{BV} is analogous to the Grashof number (Gr). No assumptions are made on the magnitude of Re_{BI} (or equivalently Re_{BV}). The effects of the orientation of gravity relative to the free-stream velocity are examined. Large deviations in the value of the drag coefficient are observed when the Froude number (Fr) decreases and/or the temperature of the sphere increases. Under appropriate constraints on Re_{BI} and Re , the total drag on a heated sphere in a low Re flow in the presence of buoyancy (mixed convection) is shown to be, within 10% error, the linear superposition of the drag computed in two canonical setups: one being the drag on a steadily moving heated sphere in the absence of buoyancy (forced convection) and the other being natural convection. However, the effect of temperature variation on the drag of a sphere in both, forced and natural convection, is significant.

I. INTRODUCTION

Natural or *free* convection is the motion of a fluid around a body caused by density gradients in the presence of gravity. Common causes for density gradients could be heat or mass transfer. Many phenomena in geophysical flows and meteorology are governed by the principles of flow resulting from density stratification in the presence of gravity. Many engineering processes like vaporization, condensation and heat transfer in packed beds rely on natural convection. This has led to many detailed studies of buoyancy driven flows [2] and their hydrodynamic stability [3]. Some exact solutions for flow in stratified fluids have also been derived [4, 5]. Similarity solutions have been derived for buoyant plumes and thermals [2, 6] while a detailed theory for the phenomena of fluid entrainment by buoyant plumes was provided by Townsend in [7].

Focusing on the case of heat transfer, temperature gradients can cause the distribution of the body force in the fluid to be non-uniform which in turn generates fluid motion. The density of the fluid in the low Mach number (Ma) limit is inversely related to the temperature via a multiplicative constant that is proportional to the thermodynamic pressure of the fluid. This dependence between density and temperature causes the fluid continuity, momentum, and energy equations to be coupled. The larger the magnitude of these temperature gradients, the stronger is the coupling between these equations. This coupling is expressed in terms of the Grashof number

(Gr) which is the ratio of the buoyancy force and the viscous force acting on a fluid. Closely related to Gr is the Rayleigh number, $Ra = GrPr$, where Pr is the Prandtl number. Coupling between the continuity, momentum, and energy equations renders their solution intractable to pen-and-paper analysis. However, some simplifying assumptions can be made when the governing parameters of the natural convection problem are constrained.

Early solutions of the coupled equations either invoked the boundary layer approximation (suitable for large values of Reynolds number (Re) and/or Gr justifying the thin boundary layer assumption while neglecting curvature effects) or linearized the governing equations paving the way for the method of matched asymptotic expansions [8]. Studies such as [9–11] focus on the limiting case of high Gr using boundary layer assumptions. Classical analytical treatments of natural convection around spheres at small Gr using matched asymptotic expansions may be found in [12–14] while experimental studies of natural convection around a heated sphere at small Gr have been conducted in [15–17] among others. These experiments were focused on measuring heat transfer and do not report measurements of drag on the sphere due to the fluid flow induced by natural convection.

A widely used set of simplifying assumptions is the Boussinesq approximation [18] which is valid when $\Delta\rho/\rho \ll 1$, where ρ denotes fluid density and $\Delta\rho$ denotes the change in density. A central theme of this paper is to study scenarios where the heat addition to a variable density fluid is not small and thus the Boussinesq approximation does not hold. Since the density is allowed to vary along with all other fluid properties, the flow does not remain incompressible but has a finite rate

* Corresponding Author. EMail: swetava@cs.stanford.edu

of dilatation.

Spjut [19] showed that the drag on a particle induced due to natural convection can be as great as the particle weight while [20–22] numerically calculated the drag due to natural convection on a heated sphere by solving the full Navier-Stokes equations in the regime where the Boussinesq approximation is valid. Dudek, et al. [23] experimentally replicated the study of [20, 21] using an electrodynamic balance.

The details of natural convective flows over surfaces and the characteristics of the resulting plume based on Gr have been studied experimentally in [24–26]. It is known from analytical solutions that in the absence of buoyancy forces ($Gr = 0$) and small Re ($Re \ll O(1)$), the effect of heat transfer can be evaluated by computing the Nusselt number (Nu) which has a value of 2. As Re increases, a Re correction is required which was evaluated by [27]. In the limit of $Gr \rightarrow 0$, both perturbation and asymptotic expansion methods have failed [27] to yield solutions for Nu with the generality of that obtained in [28] for small Peclet numbers (Pe). Boundary layer approximations have been used for large Gr [29–31].

The setup of placing a heated sphere in a uniform flow has been termed *forced* convection in literature. Many experiments and accompanying analytical studies have been carried out investigating both natural and forced convection on a variety of surfaces like spheres, flat plates, cylinders, sharp corners, and surface depressions when boundary layer approximations on these surfaces are valid. Forced convection in the absence of buoyancy with isothermal wall boundary conditions over a sphere and the resulting drag on the sphere has been studied in [1] using numerical simulations in the regime $10^{-3} \leq Re \leq 10$.

The coupled problem of placing a heated sphere in a uniform flow in the presence of gravity is called *mixed convection*. Scaling the terms in the momentum equation reveals that if $Gr/Re^2 \gg 1$, forced convection can be ignored; if $Gr/Re^2 \ll 1$, free convection can be ignored while if $Gr/Re^2 \approx 1$, the regime is that of combined forced and free convection. Depending on the domain of application and physical phenomena of interest, the effect of buoyancy can be scaled differently resulting in different non-dimensional numbers.

In geophysics, the ratio of buoyancy and flow shear terms is called the Richardson number, $Ri = (g/\rho)((\partial\rho/\partial z)/(\partial u/\partial z)^2)$, where, g is the acceleration due to gravity, ρ is the ambient fluid density, u is the fluid velocity, and z is depth. In the design of chemical process reactors and fluidized beds, the ratio of buoyancy and viscous forces on a body is called the Archimedes number, $Ar = gL^3\rho\Delta\rho/\mu^2$, where, $\Delta\rho$ is the density difference in a fluid of ambient density ρ owing to heat transfer due to a temperature difference ΔT , L is a characteristic length of the body, and μ is the fluid’s dynamic viscosity. When the density difference, $\Delta\rho$, obeys $\Delta\rho/\rho = \beta\Delta T$, where β is the volumetric thermal expansion coefficient, $Ar = Gr$ and $Ri = Gr/Re^2$. Thus, in thermal convection litera-

ture, Ri has been interpreted as the ratio of gravity forces (corresponding to natural convection) and inertia forces (corresponding to forced convection).

In mixed convection, the direction of gravity and its relative orientation with respect to the direction of the freestream velocity plays an important role. When the buoyant motion is parallel to the direction of velocity, the flow is called *aiding flow*. If the buoyant motion and forced motion are anti-parallel, the flow is called *opposing flow*. In the limit of $Re \rightarrow 0$ and $Gr = O(Re^2)$, assuming the flow is incompressible and that Boussinesq approximations hold, the effect of aiding and opposing buoyancy on creeping flow has been obtained using the method of matched asymptotic expansions by [13] and numerically by [32].

The unsteady counterpart of this problem with similar assumptions has been studied for moderate Re and small Gr such that $Gr/Re^2 \leq 40$. At higher Re , aiding flow delays the separation point further aft on the sphere while opposing flow moves the point forward [32]. Studies have documented the effects of aiding and opposing flow when $Re = O(100)$ and $O(100) < Gr < O(1000)$. Notable among these are [17, 33, 34] studying mixed convection at moderate Re and Gr on spheres, and [35, 36] studying the corresponding behavior on cylinders.

Motivated by recent interest in aerosol applications, flow features and dynamics due to mixed convection past a heated sphere have been studied numerically in the regime where Boussinesq assumptions hold for moderate Re by [37–39] while the transition to turbulence at higher Re has been investigated in [40]. The effect of Pr and Ri on mixed convection around a heated sphere at moderate Re was studied by [41] for fluids with a power-law for viscosity variation assuming small density variations so that Boussinesq assumptions hold.

It has been aptly stated in [27] that additional studies are needed to elucidate the intricate physical phenomena involved in mixed convection. In this paper, we investigate the effects of heat transfer and buoyancy on the drag of a spatially fixed heated spherical particle with isothermal wall boundary conditions in mixed convection at low Re for a variable property fluid without making any approximations or assumptions on the resulting density variation or the magnitude of heat transfer from the sphere into the fluid. It is then instructive to ask: How is the drag on a heated sphere in a slow flow modified when gravity is present? Does the drag increase or decrease? Why? How does the orientation of gravity relative to the free-stream affect the drag? Fully resolved simulations are used to quantify the effects of heat transfer and buoyancy to answer the questions posed above.

While preliminary simulations have been performed for cooled spheres, the results and analysis presented in this paper are only for heated spheres. The rest of the paper is organized as follows. Section II sets the stage by detailing the governing equations that are solved and the notation used in this paper. Section III discusses the details of the observed drag modification of a heated parti-

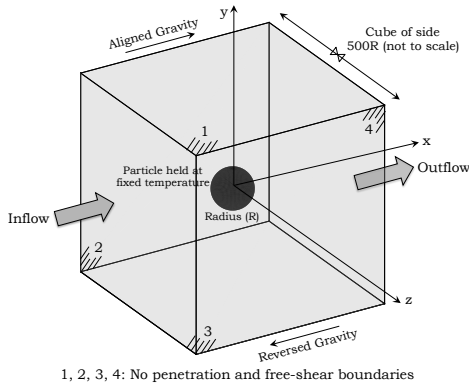


FIG. 1. A schematic of the computational setup (not to scale). All contour plots in this paper are on the xy -plane in the reference frame shown with origin at the sphere's center.

cle in the presence of buoyancy using scaling arguments, parametric studies, the qualitative impact on flow features around the particle, and the model problem of a falling sphere under the influence of gravity. Section IV summarizes the results along with concluding remarks.

II. GOVERNING EQUATIONS, NOTATION, AND NUMERICAL SOLUTION

A spatially fixed, heated spherical particle (radius R , diameter $D = 2R$) is placed in a fluid with variable density (ρ), dynamic viscosity (μ), and thermal conductivity (κ) which only vary with temperature (T_g) of the fluid. A uniform velocity, U_∞ , is prescribed far away from the fixed particle. Imposing a particle temperature, T_p , different from the ambient fluid temperature, T_∞ , at time $t = 0$, compressibility effects are important and manifest as an acoustic front at small times [42] while fluid motion occurs at much lower speed behind this front allowing for a low Mach number (Ma) limit ($Ma \rightarrow 0$) formulation of the Navier-Stokes equations [43] which is used in this paper.

The particle Biot number (ratio of heat conduction resistance to heat convection resistance) is assumed to be small ($Bi \ll 1$) implying that the particle is uniformly at the same temperature and cannot sustain any radial or angular (azimuthal or polar) gradients. Furthermore, conduction from the particle to the fluid and convection of the heat thereof is the only mode of heat transfer between the particle and the fluid. The fluid is assumed to be optically thin and in the absence of other particles, there is no scattered or incident radiation. An order of magnitude analysis [44] shows that heat transfer from the sphere due to radiation can be ignored compared to the heat transfer due to convection for the range of T_p considered in this paper. The creeping flow limit (Re is $\mathcal{O}(1)$ and smaller) is of special interest.

Assuming the fluid as air ($Pr \approx 0.7$), the full 3D, variable density, low Ma equations [43] delineated below are

solved for the fluid using the approach in [45] without making any assumption on the amount of heat addition from the sphere into the fluid or the relative magnitude of the body force with respect to the forces solely due to fluid motion (characterized by the Froude number, Fr).

$$\partial_t \rho + \partial_{x_j}(\rho u_j) = 0 \quad (1a)$$

$$\partial_t(\rho u_i) + \partial_{x_j}(\rho u_i u_j) = -\partial_{x_i} p + \partial_{x_j} \tau_{ij} + \rho g_i \quad (1b)$$

$$\tau_{ij} = \mu (\partial_{x_j} u_i + \partial_{x_i} u_j - 2/3 \delta_{ij} \partial_{x_k} u_k) \quad (1c)$$

$$\partial_t(\rho C_v T_g) + \partial_{x_j}(\rho C_p T_g u_j) = \partial_{x_j}(\kappa \partial_{x_j} T_g) \quad (1d)$$

$$P = P_0 + p = \rho R T_g \quad (1e)$$

In the above equations, u_i is the i^{th} component of the fluid velocity vector \vec{u} (the x , y , z components are also denoted by u , v , and w , respectively), p is the sum of the hydrostatic and hydrodynamic pressure, P_0 is the thermodynamic pressure, R is the ideal gas constant for air, g_i is the component of gravity in the i^{th} direction, C_v is the isochoric specific heat capacity, and C_p is the isobaric specific heat capacity. The total pressure is P where, in the low Ma limit, $p \ll P_0$. C_p and C_v are assumed to be constants.

In the limit $Ma \rightarrow 0$, the second term of the energy equation includes the pressure work term in addition to the internal energy which evaluates to the enthalpy $C_p T_g$ [43]. Heating due to viscous dissipation is negligible [46]. A power law [47] is used to model the dynamic viscosity as a function of temperature given by $\mu = \mu_0 (T_g/T_0)^n$, where μ is the viscosity at temperature T_g and μ_0 is the reference viscosity at a reference temperature T_0 . For air, $\mu_0 = 1.716 \times 10^{-5}$ kg/m-s, $T_0 = 273$ K, and $n = 2/3$. The variation of thermal conductivity is given by $\kappa(T_g) = \mu(T_g)C_p/Pr$.

It must be noted that there are other widely used correlations for μ and κ of air in the range of temperatures of interest in this paper which may be more accurate at higher temperatures and therefore induce small discrepancies in the drag values reported in this paper at these temperatures. The specific heats and Pr are also functions of temperature, albeit the variation of these quantities in the range of temperatures of interest in this paper are below 10% and will only result in small discrepancies in the drag values reported in this paper. However, these small discrepancies do not affect the analysis presented in this paper.

Figure 1 shows a schematic of the numerical setup which consists of a sphere of radius R held spatially fixed at a fixed temperature inside a cubic box large enough such that 99% of the free-stream velocity is recovered at the outlet for the Re range of interest in this paper. $(\hat{i}, \hat{j}, \hat{k})$ denote the unit vectors along the (x, y, z) axes in the reference frame shown in the figure, respectively. All contour plots in this paper are on the xy -plane in the reference frame shown with origin at the sphere's center. All descriptions of the orientation of vectors (for example, forces, gravity, velocity, etc.) are in the refer-

sumed to vary only with temperature in this paper and thus they vary only as a function of λ . These forces need to be incorporated into the total drag calculation while also assessing the partial contributions from each of the components.

A parametric study using fully resolved simulations of the heated particle is carried out to obtain the modified component-wise drag when the direction and magnitude of gravity is varied. The direction of the gravity vector may be chosen by specifying its components along the three axes in the reference frame shown in figure 1. For all computations presented in this paper, the background flow velocity is $U_\infty \hat{i}$, where U_∞ is determined by Re .

In this paper, we focus our attention on three canonical cases: (i) *Aligned Gravity*: The direction of gravity is aligned with the direction of the far-field uniform flow ($\vec{g} = |\vec{g}|\hat{i}$) and thus the flow induced by gravity opposes the background uniform flow, (ii) *Reversed Gravity*: The direction of gravity is anti-parallel to the far-field uniform flow ($\vec{g} = -|\vec{g}|\hat{i}$) and thus the flow induced by gravity aids the background uniform flow, and, (iii) *Perpendicular Gravity*: The direction of gravity is perpendicular to the direction of the far-field uniform flow ($\vec{g} = |\vec{g}|\hat{j}$). In the range of Re , λ , and Fr investigated in this paper, the direction of gravity influences the sign of the buoyancy correction term.

Although both aligned and reversed gravity setups are simulated, the aligned gravity setup is presented in more detail compared to the reversed gravity setup for brevity since the observations made in both setups are similar. Fully resolved simulations solve the full Navier-Stokes equations (1a), (1b), (1d), and (1e) in three dimensions with the body force term added.

A. Scaling the viscous pull opposite to gravity

Section 3.1 in [1] demonstrates that variable density effects are important in a fluid when $\beta_\infty \lambda T_\infty Re / \gamma_\infty \gg Ma^2$, where β_∞ is the fluid's bulk expansion coefficient evaluated at the far-field temperature. Specifically, it is shown that variable density effects are important in air. An exhaustive set of simulations, detailed in [48], were carried out to assess the steady state density changes that result around a heated sphere placed in a uniform flow in the presence of gravity as Re , λ , Fr , and the direction of gravity are varied. Figure 3 shows contour plots of the appropriately normalized density for three chosen cases while contour plots for other simulated cases are documented in [48].

It is observed that when $Re < 0.1$ and $0 \leq \lambda \leq 2$, the density field remains close to spherical (eccentricity of the contours is below 0.07) despite a three decade variation in Fr from 0.1 to 10. The temperature field mimics this behavior since in the limit $Ma \rightarrow 0$, the total pressure is almost constant and dominated by the thermodynamic pressure leading to temperature and density varying inversely following equation (1e). The small ec-

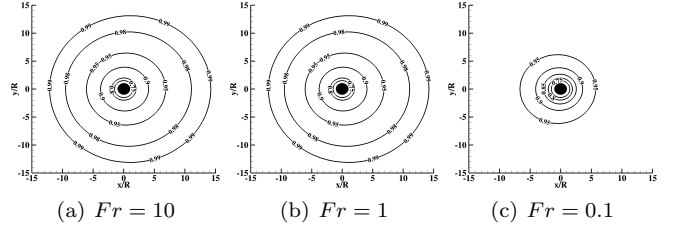


FIG. 3. Contours of normalized density, ρ/ρ_∞ , over a 3 decade variation in Fr (equivalently Re_{BI}) while Re and λ are fixed at $Re = 0.1$, $\lambda = 0.5$ in the aligned gravity setup.

centricity is a manifestation of the Oseen correction terms (small convective corrections) which are important when $r \sim \mathcal{O}(R/Re)$ (r being the radial coordinate with respect to the center of the sphere) in the absence of which, one would be solving a simple heat equation with spherically symmetric boundary conditions yielding exactly spherical contours.

This observation suggests that the convective terms in the momentum equation (1b) takes the form of linearized Oseen-like correction terms so that in the low Re , low Ma limit, the steady state momentum equation can be simplified to

$$\rho U_\infty \vec{i} \cdot \nabla \vec{u} + \nabla p = \nabla \cdot \bar{\tau} + \rho \vec{g} \quad (2)$$

where, $\bar{\tau} = \mu \left(\nabla \vec{u} + (\nabla \vec{u})^T - 2/3 (\nabla \cdot \vec{u}) \bar{I} \right)$ and \bar{I} is the identity tensor. A scaling analysis of each term in equation (2) can help understand the conditions under which these contributions balance and conditions under which a particular contribution dominates. At small Re , the Oseen correction terms are small compared to the other terms in equation (2). Assuming the orientation of gravity is either aligned or reversed compared to the background uniform flow, the buoyancy term, $B = \rho \vec{g}$, induces migration of the warm and lighter fluid in the near vicinity of the sphere in the direction opposite to \vec{g} , thereby imparting a viscous pulling force on the sphere.

Define the characteristic fluid velocities due to this induced motion as the *buoyancy induced viscous velocity*, U_{BV} , and the *buoyancy induced inertial velocity*, U_{BI} , which are obtained by scaling B with the viscous and pressure contributions in equation (2), respectively. Thus, $\lambda g \sim U_{BV} \nu_\infty / D^2 \Rightarrow U_{BV} \sim \lambda g D^2 / \nu_\infty$ and $\lambda g \sim U_{BI}^2 / D \Rightarrow U_{BI} \sim \sqrt{\lambda g D}$. Based on these velocity scales, define the *buoyancy induced viscous Reynolds number*, Re_{BV} , and the *buoyancy induced inertial Reynolds number*, Re_{BI} , as $Re_{BV} = U_{BV} D / \nu_\infty = \lambda g D^3 / \nu_\infty^2 = (Re / Fr)^2$ and $Re_{BI} = U_{BI} D / \nu_\infty = \sqrt{\lambda g D^3 / \nu_\infty} = Re / Fr$, respectively. This allows for conveniently relating all governing parameters Re , Fr , and λ of the mixed convection problem via either of Re_{BI} or Re_{BV} as $Re_{BV} = (Re / Fr)^2 = Re_{BI}^2$. Re_{BI} allows us to compress the large parametric space of Re , Fr and λ into a single parameter.

Note that the form of Re_{BV} is very similar to that of the Grashof number, Gr , which is the dimensionless number denoting the ratio of buoyancy and viscous forces and is used widely in problems involving natural convection. The Grashof number is $Gr = g\beta(T_p - T_\infty)D^3/\nu_\infty^2$ where $\beta = \beta(T) = -1/\rho(\partial\rho/\partial T)_p$ is the coefficient of thermal expansion of the fluid and is a strong function of temperature. For ideal gases, $\beta \approx 1/T_g$ and thus $Re_{BV} \approx Gr$. However, this is not true for other fluids and the functional relationship of β on T could be more complex. For this reason, we will use Re_{BV} (or equivalently Re_{BI}) instead of Gr in our analysis.

B. Mixed convection as linear superposition of forced and natural convection at low Re

A parametric study in the range $10^{-3} \leq Re \leq 10$, $0 \leq \lambda \leq 3$, and $0.1 \leq Fr \leq 10$ of the governing parameters using fully resolved simulations of the heated particle is carried out to obtain the detailed breakdown of component-wise drag in mixed convection. The corresponding cases of natural convection are also simulated while the corresponding case of forced convection is available from analysis carried out in [1]. The results from these simulations are tabulated in tables I, II, and III in section A of the appendix. Tables I and II summarize the results for aligned gravity cases while table III summarizes the results for reversed gravity. In addition to the drag in mixed convection, the tables also show the corresponding values for the drag on the sphere in forced (same Re and λ as in mixed convection) and natural convection (same λ and Fr as in mixed convection). All drag coefficient values use the inertial scaling. The qualitative observations from tables I, II, and III and linear superposition analysis presented in this section has been summarized in figure 5.

It is observed that in the regime $\{\{Re_{BI} < 0.1\} \cup \{Re_{BI} > 10\} \cup \{0.1 < Re_{BI} < 10\} \cap \{Re < 0.1\}\}$, the drag on a heated sphere in mixed convection at a given Re , λ , and Fr can be analyzed and understood as the superposition of the drag on a heated sphere in uniform flow (forced convection) with the same Re and λ as in mixed convection, and the drag on a heated sphere in natural convection in the presence of gravity at the same λ and Fr as in mixed convection. Note that the drag reported in natural convection, C_D^N is the sum of the hydrostatic component and the hydrodynamic (inertial and viscous) components. From the scaling analysis in section III A on the terms in equation (2), it is seen that the Oseen correction term scales as Re^2 , the pressure and viscous terms scale as Re while the buoyancy term scales as $Re_{BV} = Re_{BI}^2$.

Based on this scaling, we expect that when $Re < O(1)$, the Oseen correction term is small and the pressure and viscous contributions are comparable. When $Re \gg Re_{BI}^2$, the presence of gravity does not influence the total drag and thus forced convection serves as a good

approximation to mixed convection. On the other hand, when $Re \ll Re_{BI}^2$, the contribution from gravity dominates the total drag and thus natural convection serves as a good approximation to mixed convection. Our fully resolved numerical simulations corroborate these expectations as can be seen from tables I and III. The regime where $0.1 < Re_{BI} < 10$ is a regime where both forced and natural convection contributions are important and the numerical simulations help shed light on how they measure up to explain the drag in mixed convection. From the tables in section A of the appendix, it is seen that the drag on a heated sphere in mixed convection can be described within $\pm 10\%$ error by delineating three distinct regimes determined by the value of Re_{BI} .

The first regime is when $Re_{BI} < 0.1$, which is the lower extremal regime. In this regime, Fr is large compared to Re . This means that convective effects dominate and overpower buoyancy effects. Flow of the fluid around the particle is strongly modified in the presence of heat transfer from the particle as demonstrated in [1]. The drag experienced in forced convection accounts for more than 95% of the drag in mixed convection implying that drag modification is dominated by heat transfer effects compared to buoyancy effects.

The second regime is when $Re_{BI} > 10$, which is the higher extremal regime. In this regime, Fr is small compared to Re and thus the buoyancy effects overpower convective or heat transfer effects. The drag experienced in natural convection explains more than 95% of the total drag on the particle in mixed convection implying that drag modification is dominated by buoyancy effects compared to heat transfer effects. These observations are consistent with the conclusions that are drawn from the scaling argument presented above for the terms that contribute to the total drag on the particle.

The third regime is the one in between these two extremes, $0.1 < Re_{BI} < 10$. This is the regime where we have an *honest competition* between the two competing sources of drag modification. It is seen from the tables I and III that the drag in mixed convection in this regime can be explained within $\pm 10\%$ error with linear superposition of the drag from natural and forced convection when $Re \leq O(0.1)$. This is an intriguing observation and is a manifestation of the linear nature of the momentum equation (2) in the low Re , low Ma limit when the non-linear convective Oseen-like corrections are small.

At large Re , the convective terms in the momentum equation are no longer sufficiently explained by Oseen-like corrections. This implies strong, nonlinear coupling between the governing equations leading to the breakdown of the superposition hypothesis. Cases where the linear superposition breaks down due to strong nonlinear coupling between variable fluid properties and buoyancy effects are shown in table II.

We can extend the idea of linear superposition by observing that the effect of buoyancy when $Re_{BI} < 0.1$ and the effect of heat transfer when $Re_{BI} > 10$ are negligible and linear superposition also holds well in these two

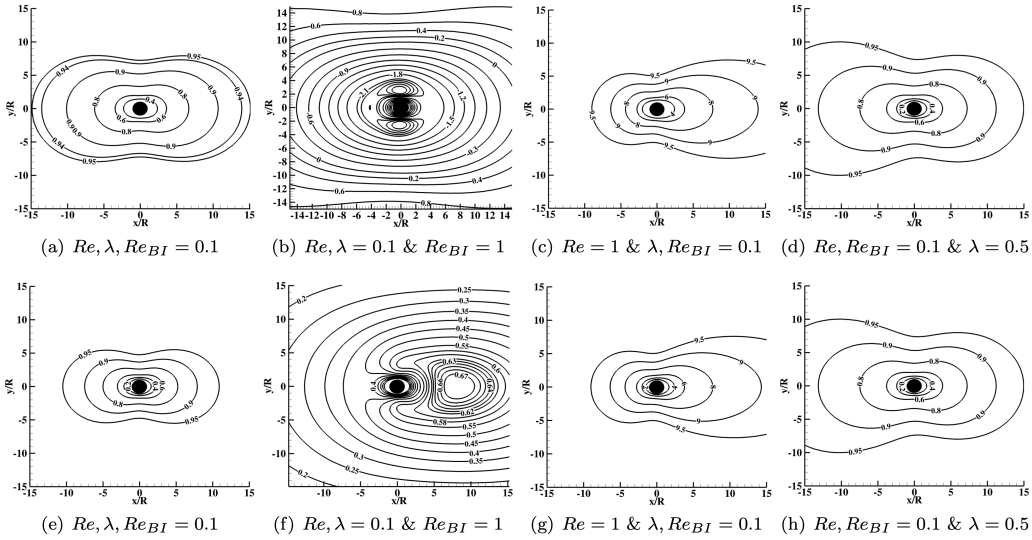


FIG. 4. Contours of normalized x -component of velocity, $u/\sqrt{\lambda g D}$. The top and bottom rows show the contours in the aligned and reversed gravity setups, respectively. Figures (a) and (e) are contours for a base case when $Re, \lambda, Re_{BI} = 0.1$. Figures (b),(f) demonstrate the effect of buoyancy by increasing Re_{BI} to 1, figures (c),(g) demonstrate convective effects by increasing Re to 1, and figures (d),(h) demonstrate heat transfer effects by increasing λ to 0.5.

regimes. The values highlighted in bold in tables I and III identify the candidates (chosen between C_D^F , C_D^N , and $C_D^F + C_D^N$) that accurately characterize the total observed drag on the sphere in mixed convection within $\pm 10\%$ error.

The success of linear superposition implies that while evaluating drag on a sphere in the low Re , low Ma limit, it is sufficient (within $\pm 10\%$ error) to use the correlations developed in [1] for a heated sphere in forced convection and the correlations or data tables developed in literature for drag on a sphere in natural convection (for example, [26]) to account for the total drag experienced by the particle. In other words, to a good approximation (within $\pm 10\%$ error), the drag modification due to heat transfer and the drag modification due to buoyancy are decoupled in this limit.

The qualitative effects of varying Re , λ , and Fr on the features of the flow can also be demonstrated by visualizing the appropriately normalized contours of the x -directional velocity component, $u/\sqrt{\lambda g D}$. Figure 4 shows the contours of $u/\sqrt{\lambda g D}$ for both aligned and reversed gravity setups. When $Fr > 1$, all effects are confined to a region about $15R$ around the particle and are therefore localized effects. However, as Re and Re_{BI} increase, the *plumelets* begin to establish a larger scale to themselves. Strong counter-rotating vortices form in the plumelet when $Fr = 0.1$ as seen in figure 4(b). Due to significant variation in fluid density, the flow is not incompressible but has finite rate of dilatation. Contours of the appropriately scaled rate of dilatation, along with contour plots of other quantities like density, temperature, and vorticity are documented in [48] and are omitted in this paper for brevity.

It is observed that as Re_{BI} increases, the density and

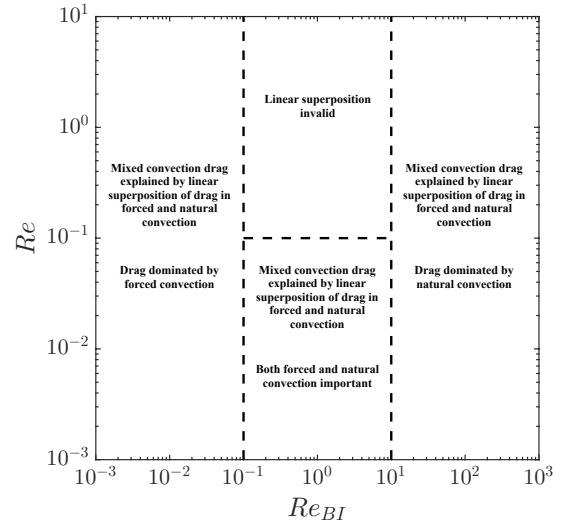


FIG. 5. Summary of linear superposition analysis of drag on a sphere in mixed convection in Re - Re_{BI} parameter space.

temperature variation becomes more concentrated near the particle. Figure 4 allows for a qualitative investigation into the individual manifestation of the effects of buoyancy, background uniform flow, and heat transfer from the particle in the flow features around the particle. It was demonstrated in [1] that while both heat transfer and convective effects increase the fore-aft asymmetry in the velocity field (in contrast to the symmetric velocity field resulting in Stokes' flow), increasing λ causes asymmetry on the anterior stagnation side of the particle while increasing Re causes asymmetry on the posterior stagnation side. This observation holds even in the presence of

gravity.

Letting figures 4(a),(e) be the base case where $Re, \lambda, Re_{BI} = 0.1$, anterior asymmetry results when λ is increased to 0.5 as seen in figures 4(d),(h) while posterior asymmetry results when Re is increased to 1 as seen in figures 4(c),(g). In section III A, it was argued that presence of gravity results in an additional force on a heated sphere due to the viscous pull caused by the migration of warm fluid near the particle in the direction opposite to gravity which scales with Re_{BI} . This fluid movement can be visualized when figures 4(a),(e) and 4(b),(f) are compared. Increasing Re_{BI} from 0.1 to 1 manifests as strong vortices near the particle that contribute to increased drag.

C. Test of decoupled drag contributions: Gravity perpendicular to background uniform flow

Encouraged by the accuracy of approximating the total drag in mixed convection as the linear superposition of the drag in forced and natural convection in the aligned and reversed gravity setups, the regime of validity of this decomposition when gravity is perpendicular to the background uniform flow is investigated in this section. This setup has also been referred to as *crossflow* in literature. With reference to the coordinate axes in figure 1, uniform flow is in the $+x$ direction while gravity is in the $+y$ direction. The Froude number in this case is the ratio of the far-field convective velocity (in the $+x$ direction) and the velocity induced due to presence of buoyancy (in the $-y$ direction).

Table IV shows the values of the x and y components of the drag in mixed convection in crossflow along with the corresponding drag values in forced and natural convection. We observe from our simulations that linear superposition holds within $\pm 10\%$ error when either (i) $Re_{BI} < 0.1$, $Re_{BI} > 10$ or, (ii) $Re \ll 1$ when $0.1 < Re_{BI} < 10$. This observation is analogous to the observation in the previous subsection.

When $Re \ll 1$, the convective terms in the momentum equation are small and negligible. These convective terms are the primary source of nonlinearities. In the absence of these terms, the momentum equation is a linear equation and coupled to the other equations only via the density. When in addition λ is small, the contributions from buoyancy and inertia linearly add to give the resultant total force on the sphere. However, even when $Re \ll 1$ but λ increases, non-Boussinesq effects become large and the linear approximation is no longer valid.

To summarize, when $Re \ll 1$ and $\lambda \rightarrow 0$, the linear superposition of the drag from forced and natural convection is a good approximation (within $\pm 10\%$ error) to the total force in mixed convection even when the body force is not parallel to the direction of the far-field imposed uniform flow. Thus, in the general case when gravity is at an angle θ with the direction of the far-field uniform flow, we can decompose the buoyancy force as having a

component $g \cos \theta$ in the direction parallel to the imposed far-field uniform flow and a component $g \sin \theta$ in the direction perpendicular to the flow. The former becomes a case of mixed convection while the latter becomes a case of natural convection. Under the constraints on Re , Fr , and λ discussed above, if linear superposition holds, then the drag due to these two components can be computed separately from the correlations and linearly superposed to obtain the total drag on the spherical particle with the error margins mentioned above.

Figure 6 qualitatively demonstrates the validity of linear superposition of the flow features of the forced and free convection problems yielding the mixed convection problem where the y -component of the velocity has been plotted for the case when $Re = 1$, $\lambda = 0.1$, and $Fr = 0.1$. Similar plots of velocity and other quantities for all the cases in table IV may be found in [48].

D. Implications for a falling heated sphere

Given the values of the drag coefficient when gravity is anti-parallel to the far-field uniform velocity in table III, one way to measure the impact of the drag modification is to compare the terminal velocity of an unheated particle (denoted by u_T^0) falling due to gravity with that of a heated particle falling under gravity, both starting from rest. Combining the analysis in [1] and this paper, we can evaluate the terminal velocity taking only heat transfer effects into consideration (denoted by u_T^H) as well as the terminal velocity taking both heat transfer and buoyancy effects into consideration (denoted by u_T^{HB}) as the parameters Re , λ , and Fr are varied. Note that u_T^0 depends only on Re , u_T^H discussed in [1] depends on Re and λ , and u_T^{HB} incorporating buoyancy effects discussed in this paper depends on Re , λ , and Fr .

If the fluid density is ρ_f , particle density is ρ_p , particle volume is V , terminal velocity of the falling particle is u_∞ , drag coefficient is C_D , acceleration due to gravity is g , and particle diameter is D , the equation [50] governing the falling particle at steady state is $u_\infty^2 C_D = (1 - \rho_f/\rho_p) g (4\rho_p D / 3\rho_f)$. If ρ_f , ρ_p , g , and D are constant, then $\xi_H = u_T^H / u_T^0 = (C_D^0 / C_D^F)^{0.5}$ and $\xi_{HB} = u_T^{HB} / u_T^0 = (C_D^0 / C_D^M)^{0.5}$. For a falling particle under the influence of gravity, C_D^M can be obtained from table III and the hydrostatic drag component removed to obey the governing equation stated above.

Evaluating ξ_H and ξ_{HB} for the parametric variation of Re , λ , and Fr denoted by the first 4 rows in table III, we obtain $\xi_H = 0.982, 0.983, 0.982$, and 0.914 , respectively, while $\xi_{HB} = 0.978, 0.981, 0.948$, and 0.887 , respectively. All values have been rounded off to 3 significant digits. As expected, the higher drag when heat transfer and buoyancy are present result in $u_T^0 > u_T^H > u_T^{HB}$. These effects are more pronounced for larger particles, smaller Fr , and larger values of λ .

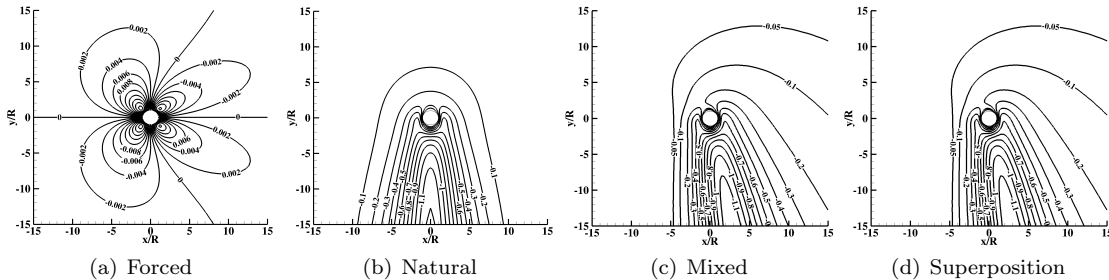


FIG. 6. Contours of y -directional velocity, $v/\sqrt{\lambda g D}$, for (a) forced convection at $Re = 1$ and $\lambda = 0.1$, (b) natural convection at $\lambda = 0.1$ and $Fr = 0.1$, (c) mixed convection at $Re = 1$, $\lambda = 0.1$, and $Fr = 0.1$, and (d) linear superposition of the forced and natural convection contours.

E. An aside on vorticity in the presence of gravity

In the case of a variable density, variable property fluid, the vorticity ($\vec{\omega}$) equation can be obtained by taking the curl of the momentum equation (1b) which at steady state becomes

$$\rho(\vec{\omega}(\nabla \cdot \vec{u}) - (\vec{\omega} \cdot \nabla)\vec{u}) = \nabla \rho \times \vec{g} + \nabla \times (\nabla \cdot \bar{\bar{\tau}}) \quad (3)$$

where, $\bar{\bar{\tau}} = \mu(\nabla \vec{u} + (\nabla \vec{u})^T - 2/3(\nabla \cdot \vec{u})\bar{\bar{I}})$ and $\bar{\bar{I}}$ is the identity tensor. For the viscous terms in equation (3) to be $\mathcal{O}(1)$, the inertial terms (convection, stretching, and tilting terms) scale as Re while the contribution from buoyancy scales as Re_{BV}/Re .

To contrast this with Stokes' flow where the particle is at the same temperature as the fluid, the vorticity equation reduces to $\nabla^2 \vec{\omega} = 0$. In the present case however, the vorticity equation has source terms owing to the contribution from buoyancy, variable density, and variable viscosity effects. Scaling analysis of equation (3) helps to revisit earlier observations in a new light as discussed below.

We observe from figures 4(b) and 4(f) that when Re_{BI} is large, the migration of the warm fluid in the near vicinity of the particle surface in the direction opposite to gravity results in the formation of a *plumelet* - a plume-like structure formed due to counter-rotating vortices in the presence of gravity which does not manifest as a full plume due to the low Re of the flow. These counter-rotating vortical structures in the plumelets become stronger as the Froude number decreases further (which is equivalent to saying that buoyancy effects become stronger and begin to dominate). From the scaling arguments presented above, it is clear that the gravitational contribution will dominate when $Re_{BV} \gg Re \implies Re \gg Fr^2$ which is consistent with our observation that the Froude number must be small for buoyancy terms to dominate.

Equation (3) also explains the validity of the low Re , low Ma , perturbation method used in [1] to explain the drag modification of a heated sphere in the limit $Re \rightarrow 0$ in the absence of buoyancy. The inertial terms that scale as Re are small and negligible in this limit. For small but

non-zero λ , equation (3) boils down to $\nabla^2 \vec{\omega} = 0$ at the first order and thus, the first order velocity correction is irrotational. The rotational part is completely contained in the Stokes-Oseen component. However, as λ increases, the velocity correction term no longer remains irrotational and the explanation power of the perturbation model starts diminishing. When $0.01 < Re < 1$ and λ is small, the source terms in the vorticity equation are small but non-negligible leading to the breakdown of the perturbation analysis.

IV. CONCLUSIONS

A quantitative and qualitative study of the effect of heat transfer and gravity on the drag and flow features of a heated sphere in the low Re and low Ma regime has been presented assuming that the sphere has small Bi . A parametric study is performed over the governing parameters of the problem namely, Re , λ , Fr , and the orientation of gravity relative to the background uniform flow. The quantitative conclusions of this parametric study are summarized in tables I, II, III, and IV. No assumptions are made on the amount of heat addition from the sphere to the fluid or the extent of density variation that takes place in the fluid.

Using scaling analysis and assuming low Re creeping flow, the ternary parametric space can be collapsed into the buoyancy induced inertial Reynolds number, Re_{BI} (or equivalently the buoyancy induced viscous Reynolds number $Re_{BV} = Re_{BI}^2$). Re_{BV} is shown to be closely related to the Grashof number. Buoyancy is shown to have a significant effect on the drag experienced by the heated sphere due to the force imparted on the sphere by the migration of the warm, low density fluid in the near vicinity of the sphere in the direction opposite to gravity. Large deviations in the value of the drag coefficient (relative to that of an unheated particle) are observed when Fr decreases (i.e. buoyancy effects dominate) and/or the temperature of the sphere increases.

When the direction of gravity is aligned with the direction of the far-field uniform flow, the drag on the sphere is reduced compared to the drag in the absence of buoyancy.

When the direction of gravity is anti-parallel to the direction of the far-field uniform flow, it enhances the drag on the sphere compared to the drag in absence of buoyancy. The parametric study also reveals that in the low Re , low Ma limit, the mixed convection problem over a heated sphere in a variable property fluid can be decomposed into two simpler canonical problems whose linear superposition explains the drag on the sphere within $\pm 10\%$ error. These canonical problems are that of drag of a heated sphere in a uniform flow in the absence of buoyancy (forced convection) and that of drag of a heated sphere in natural convection.

The linear superposition hypothesis not only holds for aiding and opposing flow, but also holds in crossflow. It is also shown that linear superposition extends to the flow features as well despite their large variation in the parametric space. The success of linear superposition is understood as a manifestation of the linear nature of the momentum equation in the low Re , low Ma limit where the convective terms are small and are sufficiently modeled by Oseen-like corrections.

Linear superposition breaks down when nonlinear coupling between variable density and buoyancy effects is significant and is characterized by the parametric space $\{0.1 < Re_{BI} < 10\} \cap \{Re > 0.1\}$.

The quantitative implication of accounting for buoyancy effects in the drag of a heated sphere falling due to gravity is evaluated by comparing its terminal velocity with that of the terminal velocity of an unheated particle. Accounting for both heat transfer and buoyancy effects results in a lower terminal velocity than accounting only for heat transfer effects due to the enhanced drag in the former case. Similar to heat transfer effects

studied in [1], buoyancy effects are more pronounced for larger particles, smaller Fr , and larger values of λ .

V. ACKNOWLEDGEMENTS

We sincerely thank Prof. Howard A. Stone for his thoughtful comments on an early draft of this paper. It is also a pleasure to acknowledge insightful discussions with members of the PSAAP II team at Stanford. This work was supported by the United States Department of Energy through the Predictive Science Academic Alliance Program II (PSAAP II) at Stanford University under grant number DENA0002373-1. All numerical simulations were performed on the Certainty Cluster at the Center for Turbulence Research at Stanford University.

Appendix A: Tables of Parametric Drag Variation

Tables I, III, and IV list the values of the total drag on a heated sphere in mixed convection when the gravity vector and the background uniform velocity vector are parallel, anti-parallel, and orthogonal, respectively and linear superposition of forced and natural convection successfully explains the drag in mixed convection within $\pm 10\%$ error. The values of drag are calculated over 3 decades of variation in both Re and Fr . Table II lists cases where linear superposition fails to explain the mixed convection drag within $\pm 10\%$ error in the aligned gravity setup.

-
- [1] S. Ganguli and S. K. Lele, Drag of a heated sphere at low reynolds numbers in the absence of buoyancy, *J. Fluid Mech.* **869**, 264 (2019).
 - [2] J. S. Turner, *Buoyancy effects in fluids* (Cambridge University Press, Cambridge, England, 1973).
 - [3] S. Chandrasekhar, *Hydrodynamic and hydromagnetic stability* (Oxford University Press, Oxford, England, 1961).
 - [4] C. S. Yih, Exact solutions for steady two-dimensional flow of a stratified fluid, *J. Fluid Mech.* **9**, 161 (1960).
 - [5] P. G. Drazin, Nonlinear internal gravity waves in a slightly stratified atmosphere, *J. Fluid Mech.* **36**, 433 (1969).
 - [6] G. K. Batchelor, Heat convection and buoyancy effects in fluids, *Quart. J. Roy. Met. Soc.* **80**, 339 (1954).
 - [7] A. A. Townsend, Entrainment and the structure of turbulent flow, *J. Fluid Mech.* **41**, 13 (1970).
 - [8] P. A. Lagerstrom, *Matched asymptotic expansions - ideas and techniques*, Applied Mathematical Series, Vol. 76 (Springer-Verlag, New York, 1988).
 - [9] H. J. Merk and J. A. Prims, Thermal convection in laminar boundary layers. I, *Appl. Sci. Res., Series A* **4**, 11 (1953).
 - [10] A. Acrivos, A theoretical analysis of laminar natural convection heat transfer to non-Newtonian fluids, *AIChE J.* **6**, 584 (1960).
 - [11] J. M. Potter and N. Riley, Free convection from a heated sphere at large Grashof number, *J. Fluid Mech.* **100**, 769 (1980).
 - [12] F. E. Fendell, Laminar natural convection about an isothermally heated sphere at small Grashof number, *J. Fluid Mech.* **34**, 163 (1968).
 - [13] C. A. Hieber and B. Gebhart, Mixed convection from a sphere at small Reynolds and Grashof numbers, *J. Fluid Mech.* **38**, 137 (1969).
 - [14] M. A. Hossain and B. Gebhart, Natural convection about a sphere at low Grashof number, in *Fourth International Heat Transfer Conference, Versailles, Paris. NCL. 6. A.I.Ch.E., New York*, Vol. 5 (1970).
 - [15] W. G. Mathers, A. J. Madden, and E. L. Piret, Simultaneous heat and mass transfer in free convection, *Ind. Engng. Chem.* **49**, 961 (1957).
 - [16] T. Tsubouchi and S. Sato, Heat transfer from fine wires and particles by natural convection, *Res. Inst. High Speed Mech., Tohoku Univ.* **12**, 127 (1960).

Re_{BI}	Re_{BV}	Re	λ	Fr	C_D^F	C_D^N	C_D^M	$100(C_D^F/C_D^M)$	$100(C_D^N/C_D^M)$	$100((C_D^F + C_D^N)/C_D^M)$
0.01	0.0001	0.1	0.1	10	253.09	-0.36	254.00	99.64	-0.14	99.50
0.1	0.01	1	0.1		28.12	-0.32	28.21	99.69	-1.13	98.56
0.1	0.01	0.1	0.1	1	253.09	-40.74	213.50	118.54	-19.08	99.46
0.1	0.01	0.1	0.5		292.34	-20.37	277.10	105.50	-7.35	98.15
0.1	0.01	0.1	1		341.99	-22.92	327.99	104.27	-6.99	97.28
1	1	0.1	0.1	0.1	253.09	-2850.27	-2613.38	-9.68	109.06	99.38
1	1	0.1	0.5		292.34	-1844.41	-1564.27	-18.69	117.91	99.22
1	1	0.1	1		341.99	-1870.39	-1551.83	-22.04	120.53	98.49
10	100	1	0.1		28.12	-1720.40	-1744.08	-1.61	98.64	97.03
10	100	1	0.5		32.66	-676.34	-676.63	-4.83	99.96	95.13
10	100	1	1		37.84	-529.92	-526.12	-7.19	100.72	93.53
100	10000	10	0.1		4.38	-1420.91	-1421.08	-0.31	99.99	99.68
100	10000	10	0.5		4.87	-354.55	-356.13	-1.37	99.56	98.19

TABLE I. Cases where linear superposition of drag on a sphere in forced and natural convection successfully explains the drag in mixed convection within $\pm 10\%$ error when gravity is parallel to the background uniform flow.

Re_{BI}	Re_{BV}	Re	λ	Fr	C_D^F	C_D^N	C_D^M	$100(C_D^F/C_D^M)$	$100(C_D^N/C_D^M)$	$100((C_D^F + C_D^N)/C_D^M)$
1	1	1	0.1	1	28.12	-29.75	1.97	1428.77	-1511.59	-82.82
1	1	1	0.5		32.66	-20.60	15.53	210.37	-132.69	77.68
1	1	1	1		37.84	-23.06	19.63	192.73	-117.45	75.28

TABLE II. Cases where linear superposition of drag on a sphere in forced and natural convection fails to explain the drag in mixed convection within $\pm 10\%$ error when gravity is parallel to the background uniform flow.

Re_{BI}	Re_{BV}	Re	λ	Fr	C_D^F	C_D^N	C_D^M	$100(C_D^F/C_D^M)$	$100(C_D^N/C_D^M)$	$100((C_D^F + C_D^N)/C_D^M)$
0.01	0.0001	0.1	0.1	10	253.09	0.36	254.29	99.53	0.14	99.67
0.1	0.01	1	0.1		28.12	0.32	28.59	98.37	1.12	99.49
0.1	0.01	0.1	0.1	1	253.09	40.74	296.95	85.23	13.72	98.95
0.1	0.01	0.1	0.5		292.34	20.37	316.48	92.37	6.44	98.81
1	1	0.1	0.1	0.1	253.09	2850.27	3138.83	8.06	90.81	98.87
10	100	1	0.1		28.12	1720.40	1784.57	1.58	96.40	97.98
100	10000	10	0.1		4.38	1420.91	1468.61	0.30	96.75	97.05

TABLE III. Cases where linear superposition of drag on a sphere in forced and natural convection successfully explains the drag in mixed convection within $\pm 10\%$ error when gravity is anti-parallel to the background uniform flow.

Re_{BI}	Re_{BV}	Re	λ	Fr	C_D^F	C_D^N	C_D^x	C_D^y	$100\sqrt{\frac{(C_D^F)^2 + (C_D^N)^2}{(C_D^x)^2 + (C_D^y)^2}}$
0.01	0.0001	0.1	0.1	10	253.09	-0.36	253.27	-0.31	99.93
0.1	0.01	1	0.1		28.12	-0.32	28.48	-0.28	98.75
0.1	0.01	0.1	0.1	1	253.09	-40.74	257.40	-29.80	98.93
1	1	1	0.1		28.12	-29.75	41.77	-21.22	87.37
1	1	0.1	0.1	0.1	253.09	-2850.27	319.91	-2846.14	99.91
10	100	1	0.1		28.12	-1720.40	177.09	-1715.48	99.77

TABLE IV. Cases where linear superposition of drag on a sphere in forced and natural convection successfully explains the drag in mixed convection within $\pm 10\%$ error when gravity is perpendicular to the background uniform flow.

- [17] T. Yuge, Experiments on heat transfer from sphere including combined natural and forced convection, *Trans. ASME* **C82**, 214 (1960).
- [18] E. A. Spiegel and G. Veronis, On the Boussinesq approximation for a compressible fluid, *J. Astrophys.* **131**, 442 (1960).
- [19] R. E. Spjut, *Heat transfer to and position control of electrostatically suspended micron-sized particles*, Ph.D. thesis (1985).
- [20] F. Geoola and A. R. H. Cornish, Numerical solution of steady-state free convective heat transfer from a solid sphere, *Int. J. Heat Mass Transfer* **24**, 1369 (1981).
- [21] F. Geoola and A. R. H. Cornish, Numerical simulation of free convective heat transfer from a sphere, *Int. J. Heat Mass Transfer* **25**, 1677 (1982).

- [22] H. Jia and G. Gogos, Laminar natural convection heat transfer from isothermal spheres, *Int. J. Heat Mass Transfer* **39**, 1603 (1996).
- [23] D. R. Dudek, T. H. Fletcher, J. P. Longwell, and A. F. Sarofim, Natural convection induced drag forces on spheres at low Grashof numbers: Comparison of theory with experiment, *Int. J. Heat Mass Transfer* **31**, 863 (1988).
- [24] F. A. M. Schenkels and J. Schenk, Dissolution of solid spheres by isothermal free convection, *J. Chem. Eng. Sci.* **24**, 585 (1969).
- [25] Y. Jaluria and B. Gebhart, On the buoyancy-induced flow arising from a heated hemisphere, *Int. J. Heat Mass Transfer* **18**, 415 (1975).
- [26] S. W. Churchill, Free convection around immersed bodies, in *Hemisphere handbook of heat exchanger design*, edited by G. F. Hewitt (Hemisphere Publishing Corporation, Taylor and Francis Group, 1990).
- [27] R. Clift, J. Grace, and M. E. Weber, *Bubbles, drops and particles* (Dover Publications, 1978).
- [28] I. Proudman and J. R. A. Pearson, Expansions at small Reynolds numbers for the flow past a sphere and a circular cylinder, *J. Fluid Mech.* **2**, 237 (1957).
- [29] A. Acrivos, Momentum and heat transfer in laminar boundary-layer flows of non-Newtonian fluids past external surfaces, *AIChE J.* **6**, 584 (1960).
- [30] W. E. Stewart, Asymptotic calculation of free convection in laminar three-dimensional systems, *Int. J. Heat Mass Transfer* **14**, 1013 (1971).
- [31] T. S. Chen and A. Mucoglu, Mixed convection about a sphere with uniform surface heat flux, *J. Heat Mass Transfer* **115:21**, 542 (1978).
- [32] S. W. Woo, *Simultaneous free and forced convection around submerged cylinders and spheres*, Ph.D. thesis, McMaster University, Hamilton, Ontario (1971).
- [33] A. Acrivos, Combined laminar free- and forced-convection heat transfer in external flows, *AIChE J.* **4**, 285 (1958).
- [34] R. S. Pearson and P. F. Dickson, Free convective effects on Stokes flow mass transfer, *AIChE J.* **14**, 903 (1968).
- [35] A. P. Hatton, D. D. James, and H. W. Swire, Combined forced and natural convection with low-speed air flow over horizontal cylinders, *J. Fluid Mech.* **42**, 17 (1970).
- [36] P. H. Oosthuizen and S. J. Madan, The effect of flow direction on combined convective heat transfer from cylinders to air, *J. Heat Transfer* **93**, 240 (1971).
- [37] E. Mograbi and E. Bar-Ziv, Dynamics of a spherical particle in mixed convection flow field, *Aerosol Science* **36**, 387 (2005).
- [38] E. Mograbi and E. Bar-Ziv, On the mixed convection hydrodynamic force on a sphere, *Aerosol Science* **36**, 1177 (2005).
- [39] M. Kotouc, G. Bouchet, and J. Dusek, Drag and flow reversal in mixed convection past a heated sphere, *Phys. of Fluids* **21**, 14 (2009).
- [40] M. Kotouc, G. Bouchet, and J. Dusek, Transition to turbulence in the wake of a fixed sphere in mixed convection, *J. Fluid Mech.* **625**, 205 (2009).
- [41] N. Nirmalkar and R. P. Chhabra, Mixed convection from a heated sphere in power-law fluids, *Chem. Engg. Sci.* **89**, 49 (2013).
- [42] S. Ganguli and S. K. Lele, Low mach, compressibility, and finite size effects of localized uniform heat sources in a gas, *Theoretical and Computational Fluid Dynamics* **33**, 341 (2019).
- [43] R. L. Panton, *Incompressible flow*, 3rd ed. (John Wiley & Sons, Inc., 2005).
- [44] For air, $\kappa = 2 \times 10^{-2} W/mK$, $T_\infty = 300K$. For particle, $D = 1\mu m$, emissivity, $\epsilon = 1$, Nusselt Number, $Nu = 2$, $T_p = 1200K$. σ_{SB} is the Stefan-Boltzmann constant. Convective thermal power, $P_c = \kappa ANu(T_p - T_\infty)/D$. Radiative thermal power, $P_r = \sigma_{SB}A(T_p^4 - T_\infty^4)$. Then $P_r/P_c = \mathcal{O}(10^{-3})$.
- [45] F. Ham, An efficient scheme for large eddy simulation of low-Ma combustion in complex configurations, Center for Turbulence Research, Annual Res. Briefs (2007).
- [46] P. K. Kundu, I. M. Cohen, and D. R. Dowling, *Fluid mechanics* (Academic Press, 2014).
- [47] W. G. Vincenti and C. H. Kruger, *Introduction to physical gas dynamics* (John Wiley and Sons, Inc., 1965).
- [48] S. Ganguli, *Computational analysis of canonical problems arising in the interaction of heated particles and a fluid*, Ph.D. thesis, Stanford University (2018).
- [49] P. A. Lagerstrom, *Laminar flow theory* (Princeton University Press, Princeton, New Jersey, 1964).
- [50] For metal particles (e.g. nickel) falling in air, $\rho_p \gg \rho_f$ so that the influence of temperature on the density ratio ρ_f/ρ_p can be safely ignored for the analysis shown here. Justifiably, we can also assume zero or negligibly small contributions from fluid inertia, added mass, and, Basset-Boussinesq history terms in the Maxey-Riley-Gatignol equation. When $Re \ll 1$, added mass factor, $\beta = 3\rho_f/(\rho_f + 2\rho_p) \ll 1$.